ELSEVIER

International Journal of Heat and Fluid Flow 19 (1998) 251–258

International Journal of HEAT AND FLUID FLOW

Forced convection cooling enhancement by use of porous materials

Y. Ould-Amer [a], S. Chikh [a], K. Bouhadef [a], G. Lauriat [b,*]

[a] *Institut de Génie Mécanique, USTHB, B.P. 32, El Alia, Bab Ezzouar 16111, Algeria*
[b] *Université de Marne-la-Vallée, Cité Descartes, Champs-sur-Marne, 77454 Marne-la-Vallée Cedex, France*

Received 25 August 1996; accepted 6 December 1997

Abstract

Results are presented for laminar forced convection cooling of heat generating blocks mounted on a wall in a parallel plate channel. The effect on heat transfer of insertion of a porous matrix between the blocks is considered. The flow in the porous medium is modeled using the Brinkman–Forchheimer extended Darcy model. The mass, momentum and energy equations are solved numerically by a control-volume-based procedure. The local Nusselt number at the walls of the blocks, the mean Nusselt numbers and the maximum temperature in the blocks are examined for a wide range of Darcy number and thermal conductivity ratio. The computations are first conducted for a single block, then for evenly mounted blocks. The results show that the insertion of a porous material between the blocks may enhance the heat transfer rate on the vertical sides of the blocks. Although the porous matrix reduces the heat transfer coefficient on the horizontal face, significant increases in the mean Nusselt number (up to 50%) are predicted and the maximum temperatures within the heated blocks are reduced in comparison with the pure fluid case.

Keywords: Forced convection cooling; Channel flow; Porous medium; Electronic cooling

Notation

c	height of the blocks
C	dimensionless height of the blocks ($C = c/H$)
c_f	fluid specific heat
Da	Darcy number ($\mathrm{Da} = K/H^2$)
e	thickness of the porous matrix
E	dimensionless thickness of the porous matrix ($E = e/H$)
F	Forchheimer coefficient in Eq. (3)
$f(d)$	function used in the energy equation
h	heat transfer coefficient
H	channel height
k_e	effective thermal conductivity
k_f	thermal conductivity of the fluid
k_s	thermal conductivity of the solid
K	permeability of the porous material
l	channel length
L	dimensionless channel length ($L = l/H$)
l_1	entrance length
L_1	dimensionless entrance length ($L_1 = l_1//H$)
l_2	length after last block
L_2	dimensionless length after last block ($L_2 = l_2/H$)
Nu	local Nusselt number
$\mathrm{Nu_b}$	mean Nusselt number for a block
p	pressure
P	dimensionless pressure ($P = p/\rho_f\ U_0^2$)
Pr	fluid Prandtl number ($\mathrm{Pr} = \nu_f/\alpha_f$)
q	heat dissipation per cubic meter ($q = Q/cw$)
Q	heat dissipation per unit length in each block
Re	Reynolds number ($\mathrm{Re} = \rho_f U_0 H/\mu_f$)
R_k	thermal conductivity ratio (k_s/k_f or k_e/k_f)
s	spacing between the blocks
S	dimensionless spacing between the blocks ($S = s/H$)
T'	temperature
T	dimensionless temperature ($T = (T' - T_0/(Q/k_f))$
T_0	inlet temperature
u	axial velocity
U	dimensionless axial velocity ($U = u/U_0$)
U_0	uniform inlet velocity
v	transverse velocity
V	dimensionless transverse velocity ($V = v/U_0$)
w	block width
W	dimensionless block width ($W = w/H$)
x	axial coordinate
X	dimensionless axial coordinate ($X = x/H$)
y	transverse coordinate
Y	dimensionless transverse coordinate ($Y = y/H$)

Greek

α	thermal diffusivity ($\alpha = k/\rho_f c_f$)
ε	porosity
Φ	general dependant variable
λ	inertial coefficient ($\lambda = F\varepsilon/\mathrm{Da}^{1/2}$)

* Corresponding author.

0142-727X/98/$19.00
PII: S0142-727X(98)00004-6

μ dynamic viscosity
ν kinematic viscosity
ψ stream function
ρ density

Subscripts
b averaged over the block
e effective property of the porous medium
f fluid
p porous
s solid
w wall

Superscript
′ dimensional temperature

1. Introduction

As it is known, humidity, dust and vibrations are among the causes of failure of electronic components, but overheat is the most important cause. Although the heat dissipated in many electronic devices is moderate, for example about 100 W for computer CPU's, the overall volumetric heat generation may be considerable and the power density can reach megawatts per cubic meter caused by the compacity of electronic equipments.

The need for higher speed clocks, for noise reduction (by reducing the use of fans) and the increasing use of Multi-Chip-Modules (MCM) are as many additional constraints from the thermal point of view. Thus, the improvement of the heat removal capacity is a major concern for the designers in order to keep the operating temperature below an allowable level.

Conventional cooling techniques involving natural or forced convection heat transfer are frequently employed. However, these techniques are not sufficient in many situations to evacuate enough heat. A literature survey shows that a great amount of work has been done on this topic. A review of theoretical and experimental works on the thermal control of electronic equipment has been made by Peterson and Ortega (1990). Zebib and Wo (1985) studied a two-dimensional forced convection air cooling of a single heated block mounted on the wall of a horizontal channel. In their work on forced convection of an array of heat generating rectangular blocks, Davalath and Bayazitoglu (1987) showed that the vertical faces are not efficiently cooled. Afrid and Zebib (1989, 1991) investigated numerically a two-dimensional conjugate conduction-natural convection cooling of mounted blocks on an insulated vertical plate, and a three-dimensional laminar and turbulent natural convection cooling of heated blocks. They concluded in the first paper that increasing the spacing between the heated blocks led to a better cooling. In the second paper, they showed that there exists a qualitative similarity of the flow and thermal fields of the laminar and turbulent models. However, smaller temperatures are obtained with the turbulent model which is in good agreement with experimental results. Experimental works were conducted by Ortega and Moffat (1985) and Moffat and Ortega (1986a, b) on free convection and buoyancy induced forced convection using a system of ten rows and eight columns of aluminum cubes mounted on an insulated plate. Anderson and Moffat (1988) and Moffat and Anderson (1988) presented experimental studies on forced convection cooling with the same geometry as in Ortega and Moffat (1985). Keshavarz et al. (1995) studied numerically a combined free and forced convection laminar flow problem in a parallel plate channel with surface mounted ribs. They investigated the effect of suction and injection of cold fluid through a small hole pierced after each rib. They concluded that the local Nusselt numbers on the side walls are higher than along the top wall at low Reynolds numbers. Composite fluid-porous systems have been also studied by several authors. Partially porous channels or ducts have been considered by Poulikakos and Kazmierczak (1987) and Chikh et al. (1995a, b). They showed that the thickness of the porous layer has a strong effect on the heat transfer coefficient. In their study, Huang and Vafai (1994) considered a forced convection problem in an isothermal parallel plate channel with porous blocks using a vorticity stream function formulation. They showed that significant heat transfer augmentation can be achieved through the use of multiple emplaced porous blocks.

The present work deals with the problem of heat transfer enhancement by forced convection at the vertical walls of heat generating blocks evenly mounted on the lower plate of a channel through the insertion of porous materials between the blocks. A numerical study is carried out using a control volume method. The flow field is governed by the Navier–Stokes equations in the fluid region, the Darcy–Brinkman–Forchheimer equation in the porous region, and the thermal field by the energy equation. The heat transfer results are discussed in terms of Nusselt numbers and maximum temperatures reached within the blocks.

2. Mathematical formulation

The physical domain and coordinate system are shown in Fig. 1. A two-dimensional, laminar, incompressible, steady flow of a Newtonian fluid with constant properties takes place in both fluid and porous regions, bounded by two adiabatic plates. The fluid enters the channel with uniform velocity

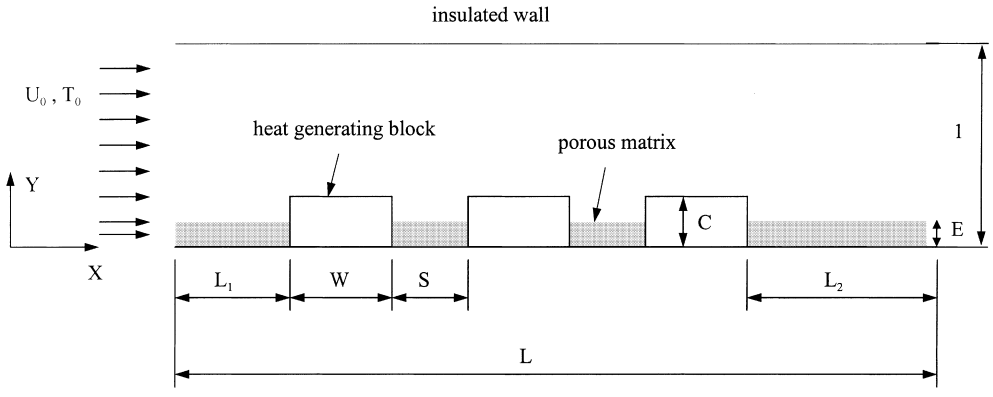

Fig. 1. Schematic of the physical domain.

and temperature. The flow is modelled by the Darcy–Brinkman–Forchheimer equation in the porous matrix in order to account for inertia and boundary effects and by the Navier–Stokes equations in the fluid domain. Evenly spaced solid blocks, which occupy 25% of the channel height, are mounted on the lower wall. The heat generation within the blocks is assumed to be constant and uniform. The porous material is assumed to be homogeneous, isotropic and saturated with a single phase fluid that is in local thermal equilibrium with the solid matrix. The conservation equations for mass, momentum and energy are written as follows:

Mass:

$$\nabla \cdot \vec{v} = 0. \tag{1}$$

Momentum:

In the fluid region:

$$\vec{v} \cdot \nabla \vec{v} = -\frac{1}{\rho_f} \nabla p + \nu_f \nabla^2 \vec{v}. \tag{2}$$

In the porous medium (Vafai and Tien, 1981):

$$\frac{1}{\varepsilon}(\vec{v} \cdot \nabla \vec{v}) = -\frac{1}{\rho_f} \nabla p - \frac{\nu_f}{K} \vec{v} - \frac{F\varepsilon}{K^{1/2}} |\vec{v}| \vec{v} + \frac{\nu_f}{\varepsilon} \nabla^2 \vec{v}. \tag{3}$$

Energy:

In the fluid region:

$$\rho_f c_f (\vec{v} \cdot \nabla T') = k_f \nabla^2 T'. \tag{4}$$

In the porous medium:

$$\rho_f c_f (\vec{v} \cdot \nabla T') = k_e \nabla^2 T'. \tag{5}$$

In the solid blocks:

$$k_s \nabla^2 T' + q = 0. \tag{6}$$

The governing equations are made dimensionless by adopting the following nondimensional quantities:

$$X = \frac{x}{H}, \qquad Y = \frac{y}{H}, \qquad \vec{V} = \frac{\vec{v}}{U_0}, \qquad T = \frac{T' - T_0}{Q/k_f},$$

$$P = \frac{P}{\rho_f U_0^2}.$$

The governing equations are then written in compact forms as:

Mass:

$$\nabla \cdot \vec{V} = 0. \tag{7}$$

Momentum:

$$\frac{1}{\varepsilon}(\vec{V} \cdot \nabla \vec{V}) = -\nabla P + \frac{1}{\varepsilon\ \mathrm{Re}} \nabla^2 \vec{V} - \frac{1}{\mathrm{Re\ Da}} \vec{V} - \lambda |\vec{V}| \vec{V}, \tag{8}$$

where λ is the inertial coefficient equal to $(F\varepsilon/\mathrm{Da}^{1/2})$. In the fluid region, Da is set to infinity and ε to unity in order to transform Eq. (8) to Navier–Stokes equation. In the blocks, $\mathrm{Da} = 0$; this yields $\vec{V} = \vec{0}$. We consider highly porous materials, such as foams, with a porosity close to unity.

Energy:

$$\vec{V} \cdot \nabla T = \frac{R_k}{\mathrm{Re\ Pr}} \nabla^2 T + \frac{f(d)}{\mathrm{Re\ Pr}\ CW}, \tag{9}$$

where R_k is the thermal conductivity ratio defined as:

$$R_k = \begin{cases} k_s/k_f & \text{in the solid blocks (taken equal to 10 in} \\ & \text{the present study),} \\ 1 & \text{in the fluid domain,} \\ k_e/k_f & \text{in the fluid saturated porous medium,} \end{cases}$$

$f(d)$ is a function set equal to one to account for heat generation in the blocks, and to zero elsewhere. A model between the series and parallel models may be used for the effective thermal conductivity of the porous material. However, in this study we focus on the magnitude of k_e.

The conditions at the channel inlet are uniform velocity and temperature profiles. At the exit, the downstream length L_2 was chosen long enough to ensure that the velocity profile is fully developed, and to neglect axial conduction. At the impermeable walls, no slip boundary conditions are applied. The top and bottom walls are considered adiabatic. To handle the abrupt changes in thermophysical properties within the calculation domain (solid, porous, fluid), the harmonic mean is used to evaluate the properties at different interfaces.

The relevant dimensionless boundary conditions are:

$$\text{at } X = 0,\ 0 < Y < 1, \qquad U = 1, \quad V = 0, \quad T = 0, \tag{10}$$

$$\text{at } X = L,\ 0 < Y < 1, \qquad \frac{\partial U}{\partial X} = 0, \quad V = 0, \quad \frac{\partial T}{\partial X} = 0, \tag{11}$$

$$\text{at } Y = 0, 1,\ 0 < X < L, \qquad U = 0, \quad V = 0, \quad \frac{\partial T}{\partial Y} = 0. \tag{12}$$

In the above system of equations, the following nondimensional parameters emerge:

$$\mathrm{Da} = \frac{K}{H^2}, \qquad \mathrm{Re} = \frac{\rho_f U_0 H}{\mu_f}, \qquad \mathrm{Pr} = \frac{\nu_f}{\alpha_f}, \qquad C = \frac{c}{H},$$

$$W = \frac{w}{H}.$$

3. Numerical procedure

A control volume method was utilized to solve the conservation equations using a pressure–velocity formulation. A staggered grid was considered such that the velocity components are located at the control volume faces whereas pressure and temperature are located at the centers of control volumes as suggested by Patankar (1980). The sudden change in the diffusion coefficients (viscosity or thermal conductivity) was handled by use of the harmonic mean to ensure conservation and uniqueness of mass and heat fluxes at each control volume face.

The SIMPLE algorithm was adopted to solve for the flow field. The algebraic equations were solved using a line by line technique, combining between the tridiagonal matrix algorithm and the Gauss–Seidel method. Because of the nonlinearities in the momentum equations, the velocity components were under-relaxed. The convergence of computations was assumed to be achieved when the equation of continuity was satisfied to three significant digits and when the residual (absolute value of relative error in velocity components at each grid point) was found to be less than 10^{-5}.

A nonuniform grid with a large concentration of nodes close to the walls and blocks was employed. A 100×50 mesh was chosen, with a finer grid near the solid boundaries. The effect of the grid size on the average Nusselt number for each block is shown in Table 1. The results are shown to differ only by 1.2% for the case $\mathrm{Re} = 1000$, $\mathrm{Da} = 10^{-3}$ and $k_e/k_f = 100$. Therefore, the 100×50 grid used appears to be sufficiently fine to provide accurate results for engineering purposes.

To validate the computer code, comparisons with the published results of Davalath and Bayazitoglu (1987) were made. The average Nusselt number over each block was computed with our code by setting $\mathrm{Da} \to \infty$, for $\mathrm{Re} = 100$ and 1000 using a parabolic inlet velocity profile. Fig. 2 shows a good agreement between the two studies. The small differences (about 6% at $\mathrm{Re} = 1000$ for the first block) are mainly due to the upwind scheme used by Davalath and Bayazitoglu (1987) which causes a false diffusion, especially at the leading edge and the trailing edge of the first and last blocks respectively. It is worth noting that a developing velocity profile yields slightly higher local Nusselt numbers on the frontal face of

Table 1
Effect of the mesh size on average Nusselt number for Re $=1000$, Da $=10^{-3}$, $\lambda = 0.35$, Pr $=0.7$ and $k_e/k_f = 100$

Number of nodes	Average Nusselt number (Nu_b)		
	First block	Second block	Third block
100×50	929.83	183.28	169.47
160×58	929.60	184.15	168.91
200×100	931.77	182.66	167.35
Maximum relative error (%)	0.2	0.8	1.2

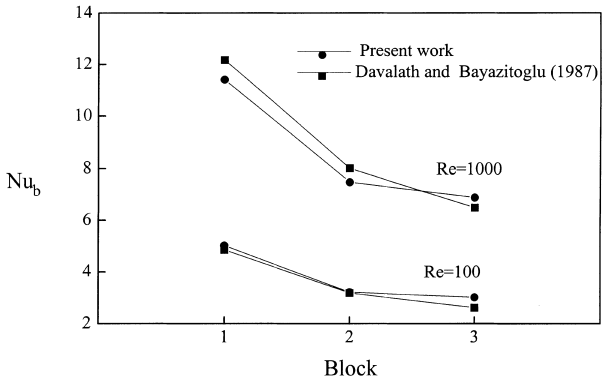

Fig. 2. Comparisons of mean Nusselt numbers with previously published results.

the first block due to a greater cross-stream velocity component, in comparison with a fully developed parabolic velocity profile. However, the differences do not exceed 5%.

4. Results and discussion

Due to the great number of parameters, few of them were kept constant. All the computations were conducted for air (Pr $=0.7$), a porosity $\varepsilon = 1$ and a thermal conductivity ratio of the blocks $k_s/k_f = 10$ which is a representative value for semi-conductors. Block dimensions and spacing were: $C = 0.25$, $W = 0.5$, $S = 1$, $L_1 = 1$ and $L_2 = 20$.

In the first part, the analysis is carried out for the case of a single block mounted in the channel. The effects of an inserted porous matrix (with $E = 0.25$) on the Nusselt number and temperature are analyzed.

The local Nusselt number along the surface of the blocks is defined as in Davalath and Bayazitoglu (1987):

$$\mathrm{Nu} = \frac{hH}{k_f} = -\frac{R_k \partial T/\partial \mathbf{n}|_w}{T_w}, \tag{13}$$

n being the unit normal to the interface between the block and the fluid, and T_w the wall temperature. It should be pointed out that the mean temperature of the fluid does not appear because it was assumed to be too small in comparison with the wall temperature, due to heat generation in the blocks.

The mean Nusselt number for a block is evaluated as follows:

$$\mathrm{Nu}_b = \frac{1}{A}\int_A \mathrm{Nu}\, dA, \tag{14}$$

where A is the surface area of the block exposed to the fluid.

Fig. 3 shows the local Nusselt number distribution on the different walls for highly conducting ($k_e/k_f = 100$) and for

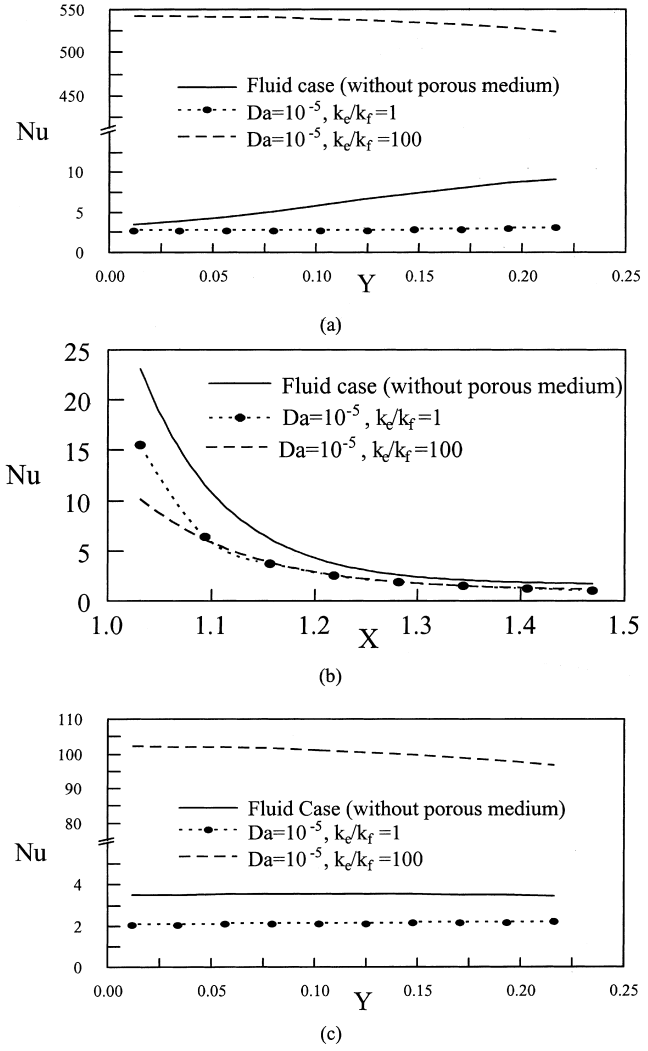

Fig. 3. Local Nusselt number on the three walls of the block for Re $=750$, $E = 0.25$ and $\lambda = 0.35$.

low conducting ($k_e/k_f = 1$) porous materials with a dimensionless height $E = 0.25$, and for the case without porous medium. On the side walls (Fig. 3(a) and (c)), the porous matrix constitutes a resistance to the flow. Therefore, the convection heat transfer is reduced along the side walls. However, if the effective thermal conductivity of the porous material is high enough the conductive heat transfer is increased and the total heat transfer is higher than for the fluid case at both frontal and rear vertical faces. On the other hand, the presence of the porous matrix reduces the heat transfer coefficient on the top wall in comparison with the fluid case whatever the value of the effective thermal conductivity, as illustrated in Fig. 3(b).

The temperature field inside the solid block is presented in Fig. 4 for $k_e/k_f = 100$, Da $=10^{-2}$ and 10^{-5}. For this case of a highly conducting porous material, it is shown that the heat transfer is enhanced in comparison with the fluid case. A 56% reduction in the maximum temperature at the block is obtained for the more permeable and conducting case (Da $= 10^{-2}, k_e/k_f = 100$). Moreover, it is observed that the region in which the temperatures are the highest moves toward the center of the block. This is due to a better cooling of the side walls.

In what follows, three blocks are considered. The streamlines are first presented in Fig. 5 for different permeabilities

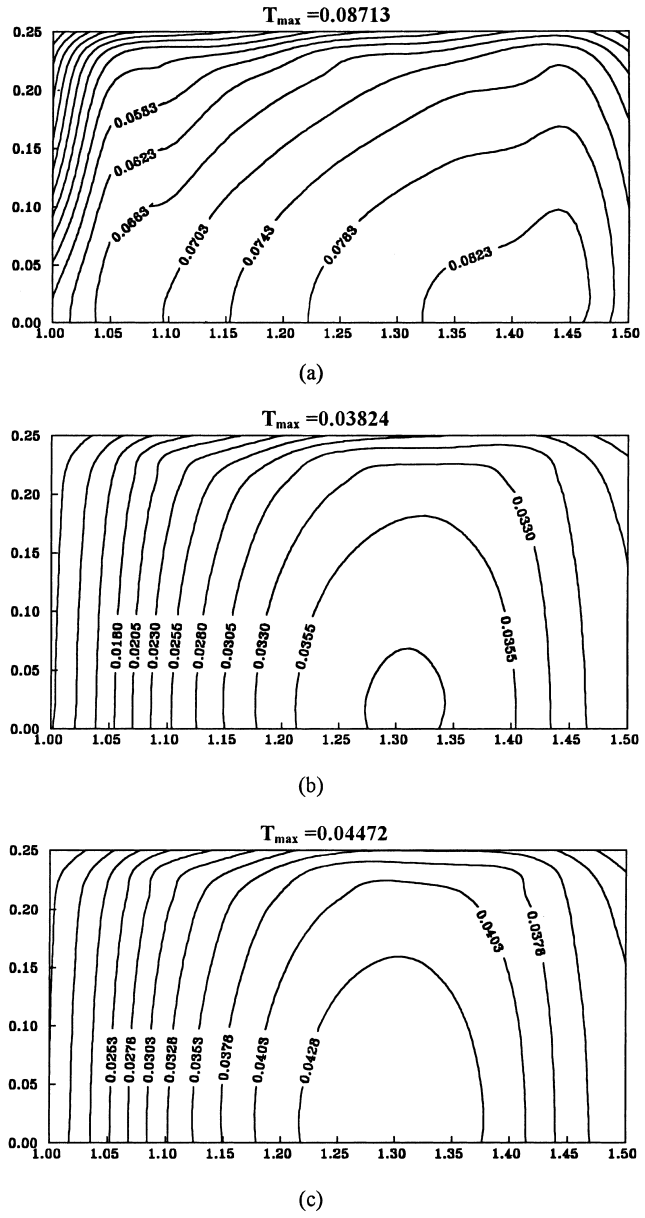

Fig. 4. Dimensionless temperature contours within the block for Re $=750$ and $E=0.25$.

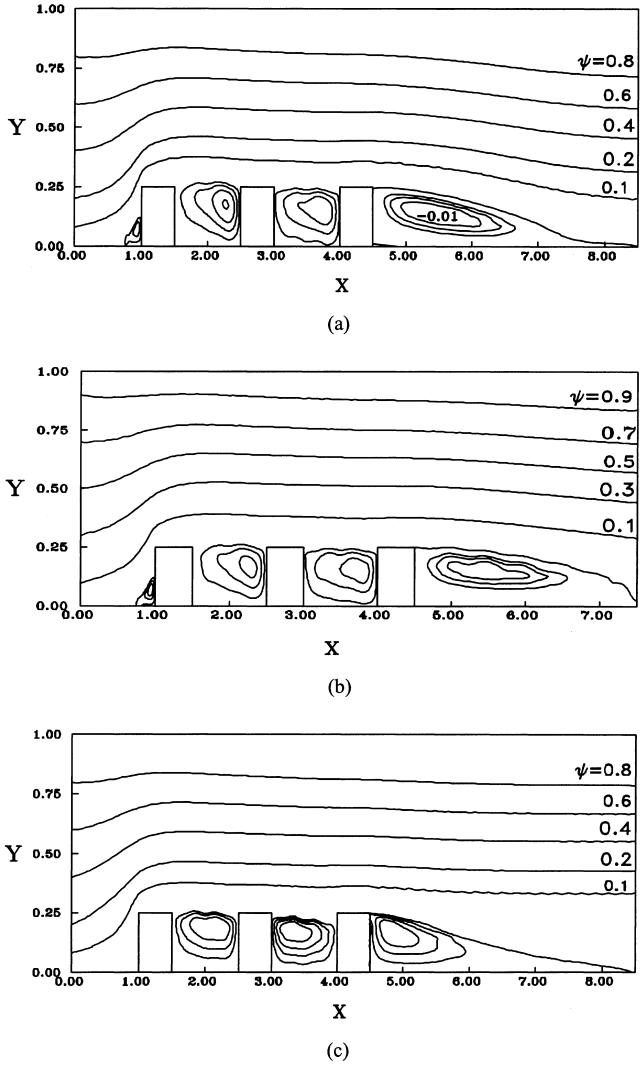

Fig. 5. Streamlines for Re $=1000$ and $E=0.25$.

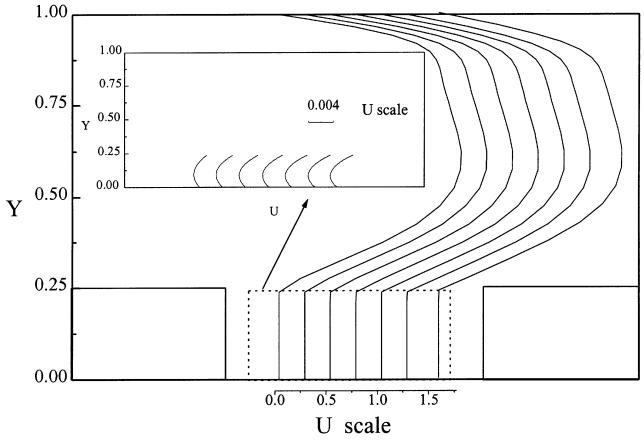

Fig. 6. Axial velocity profiles between two blocks for Re $=1000$, Da $=10^{-5}$, $E=0.25$ and $\lambda=0.35$.

of the porous material which occupies 25% of the channel height ($E=C$). As Da decreases, the recirculation zone in front of the first block tends to disappear and the vortex after the last block decreases in length. The axial velocity profile between the first two blocks is shown in Fig. 6. It may be noticed that the velocity magnitude in the porous region is much lower than in the plain zone. The local Nusselt number distributions at the walls of the three blocks are presented in Fig. 7 for $E=0.25$, Da $=10^{-5}$ and $k_e/k_f=100$. As in the case of a single block, it was found that the heat transfer on the side walls is augmented by the porous matrix while the local Nusselt number is reduced on the horizontal faces. It can also be seen that Nu is higher at the frontal vertical face of the first block (AB) and decreases for the next two blocks (EF, IJ), since the fluid is heated when it flows through the channel.

Due to the fluid motion in the reversed flow regions, the frontal side of a block is cooled before the rear side of the previous block: EF is cooled before CD and IJ is cooled before GH. This flow reversal explains that the Nusselt number is the highest for the side wall KL because there is no heat

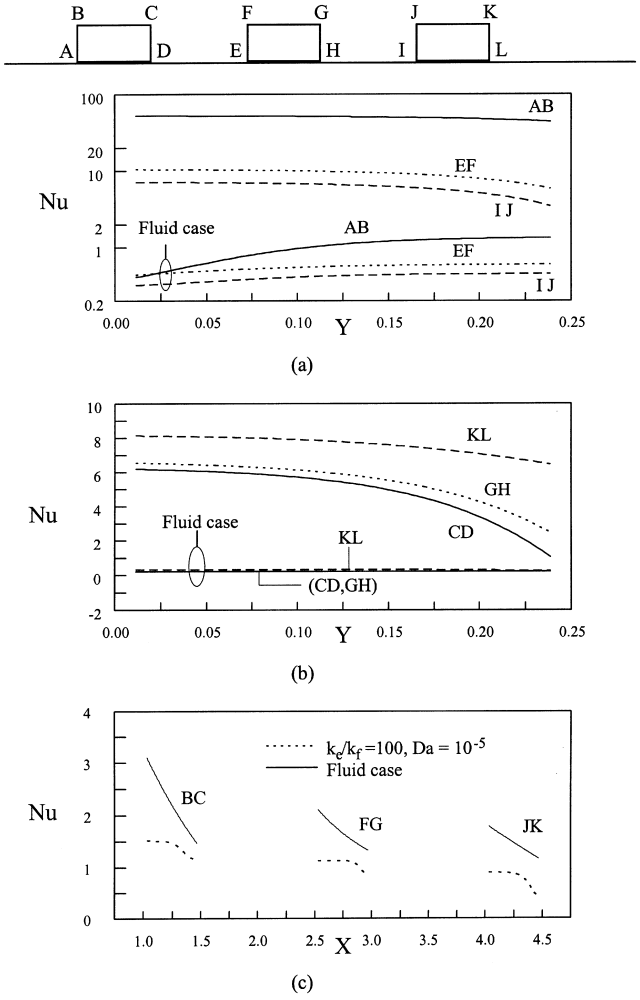

Fig. 7. Local Nusselt number on the walls of the three blocks for Re = 1000, Da = 10^{-5}, $\lambda = 0.35$, $E = 0.25$ and $k_e/k_f = 100$.

generating block behind this wall. Fig. 8 shows that the insertion of a porous material between the blocks lead to an increase in the total heat transfer rate at the three blocks. The isotherms within the third block are presented in Fig. 9. This block remains the least cooled one when the Darcy number is increased from the solid case (Da = 0) to the fluid case (Da→ ∞). It can be seen that the fluid case (Fig. 9(d)) is less

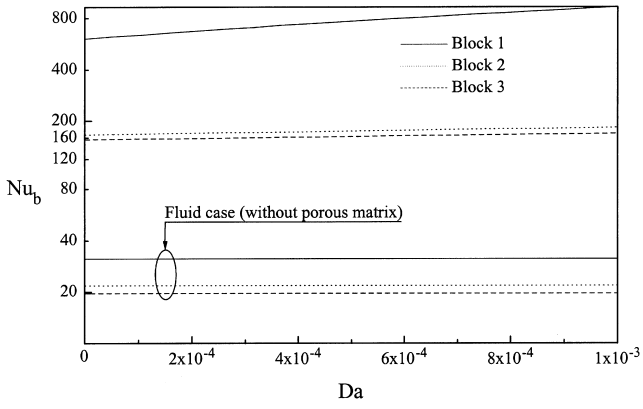

Fig. 8. Mean Nusselt number on each block as a function of Da for Re = 1000, $E = 0.25$, $\lambda = 0.35$ and $k_e/k_f = 100$.

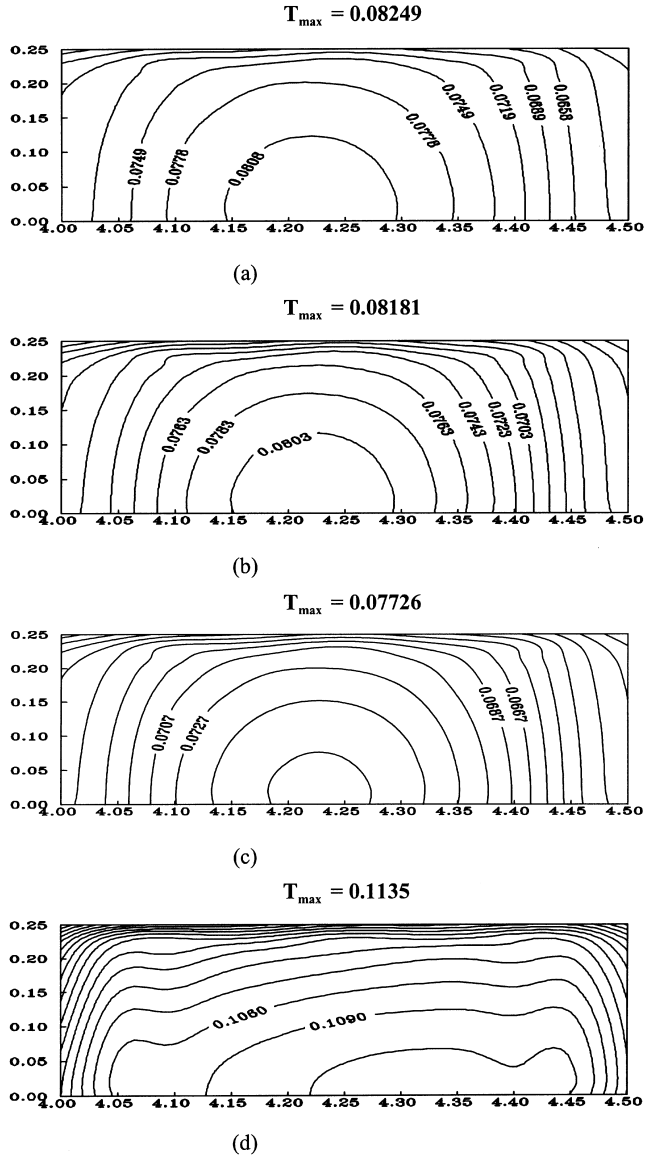

Fig. 9. Dimensionless temperature contours within the last block for Re = 1000, $E = 0.25$ and $\lambda = 0.35$.

efficient since the maximum temperature reached in the block is the highest. It is also shown that the fluid motion in a porous material of highly effective thermal conductivity (Fig. 9(b) and (c)) enhances the heat transfer rate in comparison with the two limiting cases of pure conduction (Fig. 9(a)) and fluid convection with flow reversal (Fig. 9(d)).

The effects of the thermal conductivity ratio on the Nusselt number and temperature fields are presented in Figs. 10 and 11. As expected, the Nusselt number is increased (Fig. 10) with the effective thermal conductivity of the porous medium and a sharp increase is shown for moderate values of the conductivity ratio due to the flow resistance caused by the porous medium. In addition, Fig. 11 shows that the maximum temperature in the last block may be reduced by up to 34% in comparison with the pure fluid case. The effect of the dimensionless height of the porous material (E) on the mean Nusselt number for each of the blocks is presented in Fig. 12 for $k_e/k_f = 100$ and Da = 10^{-5}. For this case of highly conducting material, the presence of the porous matrix enhances the heat transfer for

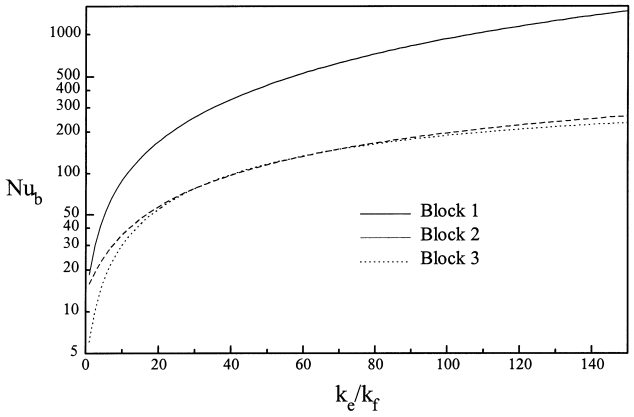

Fig. 10. Mean Nusselt number at each block versus k_e/k_f for Re $=1000$, Da $=10^{-3}$, $E=0.25$ and $\lambda=0.35$.

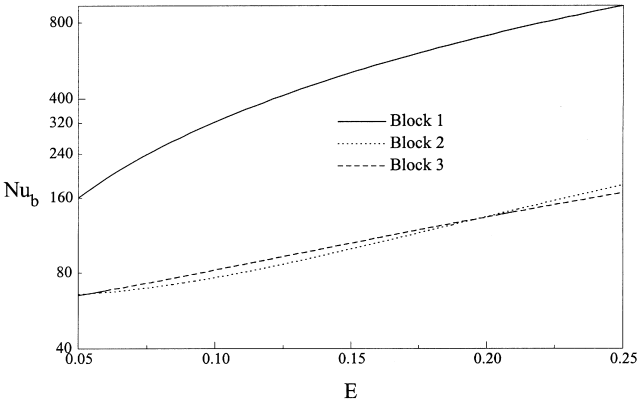

Fig. 12. Mean Nusselt number for each of the three blocks as a function of the dimensionless thickness of the porous insertion for Re $=1000$, Da $=10^{-3}$, $\lambda=0.35$ and $k_e/k_f=100$.

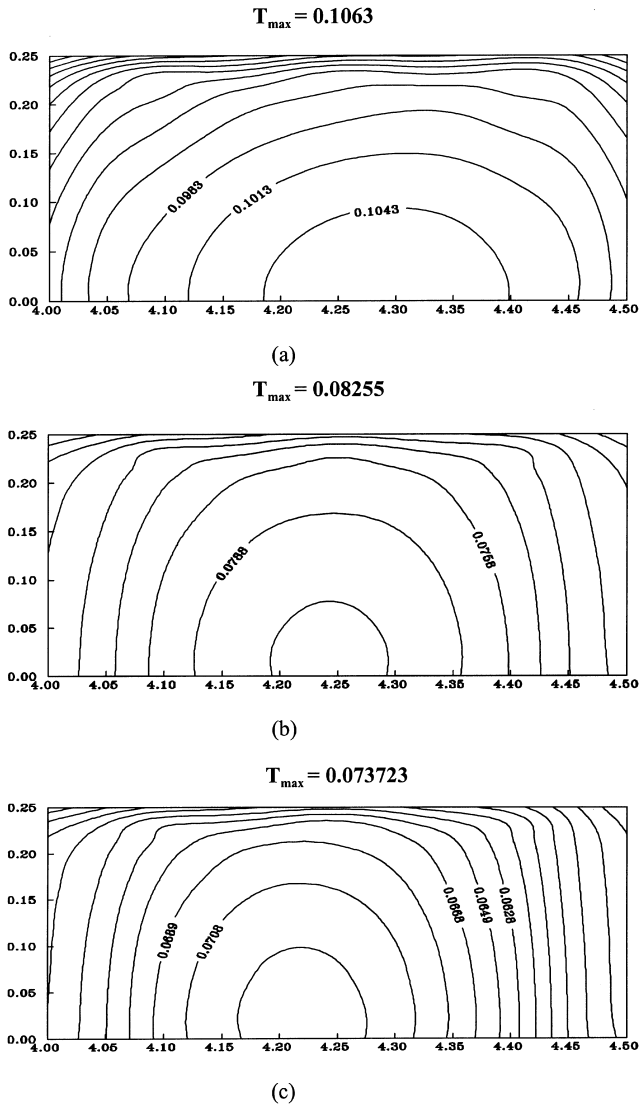

Fig. 11. Dimensionless temperature contours within the last block versus k_e/k_f for Re $=1000$, Da $=10^{-3}$, $E=0.25$ and $\lambda=0.35$.

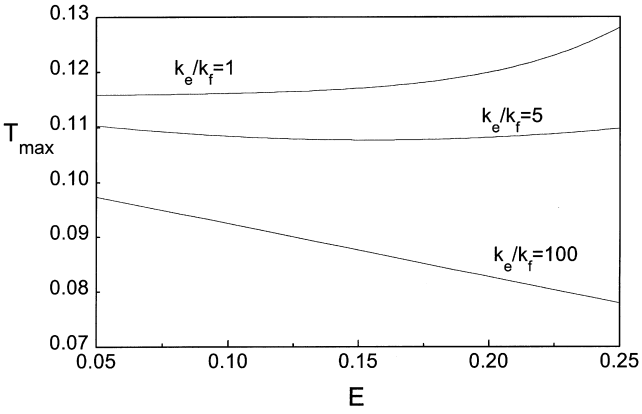

Fig. 13. Maximum dimensionless temperature in the last block as a function of the dimensionless thickness of the porous insertion for Re $=1000$, Da $=10^{-3}$ and $\lambda=0.35$.

the three blocks and the thicker is the porous layer, the higher is the mean Nusselt number. However, the variations of the maximum temperature in the last block as a function of the porous height for various conductivity ratios (Fig. 13) show an opposite effect for small thermal conductivity ratios. For $k_e/k_f=1$, the porous layer can be considered as a resistance to the flow which has the effect of reducing the heat transfer. Therefore, an increase in E produces higher temperatures in the block. If the porous material has a moderate thermal conductivity ($k_e/k_f=5$), an optimal thickness exists at which the maximum temperature reaches a minimum value. Further increases in E cause a decrease in the flow rate inside the porous material and the augmentation of conductive heat transfer does not compensate the reduction in convective heat transfer. For highly conducting porous matrix ($k_e/k_f=100$), an increase in the porous material thickness systematically produces a decrease in T_{max} since the conductive heat transfer predominates.

5. Conclusion

A numerical study of laminar forced convection cooling of heat generating blocks evenly mounted in a parallel plate channel was carried out. It is shown that the side walls of the blocks are not well cooled when using conventional tech-

niques due to flow recirculations. Insertion of porous materials between the blocks produces an enhancement of the cooling of the blocks provided that the effective thermal conductivity of the porous medium is much higher than the fluid conductivity. The maximum temperature inside the block decreases all the more since the permeability of the porous medium is low.

References

Afrid, M., Zebib, A., 1989. Natural convection cooling of heated components mounted on a vertical wall. Numer. Heat Transfer A 15, 243–259.

Afrid, M., Zebib, A., 1991. Three-dimensional laminar and turbulent natural convection cooling heated blocks. Numer. Heat Transfer A 19, 405–424.

Anderson, A.M., Moffat, R.J., 1988. Direct air cooling of electronic components: Reducing component temperatures by controlled thermal mixing. Paper presented at ASME/WAM Conference, Chicago, IL, 27 November–2 December.

Chikh, S., Boumedien, A., Bouhadef, K., Lauriat, G., 1995a. Analytical solution of non-Darcian forced convection in an annular duct partially filled with a porous medium. Int. J. Heat Mass Transfer 38, 1543–1551.

Chikh, S., Boumedien, A., Bouhadef, K., Lauriat, G., 1995b. Non-Darcian forced convection in an annulus partially filled with a porous material. Numer. Heat Transfer A 28, 707–722.

Davalath, J., Bayazitoglu, Y., 1987. Forced convection cooling across rectangular blocks. J. Heat Transfer 109, 321–328.

Huang, P.C., Vafai, K., 1994. Analysis of forced convection enhancement in a channel using porous blocks. J. Thermophys. Heat Transfer 8, 563–573.

Keshavarz, A., Shahmardan, M.M., Mansouri, S.H., Rahnama, M., 1995. Numerical investigation of combined free and forced convection laminar flow between parallel plates channel with surface mounted ribs. In: Lewis, R.W., Durbetaki, P. (Eds.), Numerical Methods in Thermal Problems, IX, Part 1, Pineridge, Swansea, pp. 169–177.

Moffat, R.J., Anderson, A.M., 1988. Applying heat transfer coefficient data to electronic cooling. Paper presented at the ASME/WAM Conference, Chicago, IL, 27 November–2 December.

Moffat, R.J., Ortega, A., 1986a. Buoyancy Induced forced convection. AIAA/ASME Thermophysics and Heat Transfer Conference, Boston, Mass., 2–4 June.

Moffat, R.J., Ortega, A., 1986b. Buoyancy induced convection in an non-uniformly heated array of cubical elements on a vertical channel wall. AIAA/ASME Thermophysics and Heat Transfer Conference, Boston, Mass., 2–4 June.

Ortega, A., Moffat, R.J., 1985. Heat transfer from an array of simulated electronic components: Experimental results for free convection with and without shrouding wall Heat Transfer in electronic equipment. ASME HTD, vol. 48.

Patankar, S.V., 1980. Numerical Heat Transfer and Fluid Flow. Mc Graw-Hill, New York.

Peterson, G.P., Ortega, A., 1990. Thermal control of electronic equipment and devices. Adv. Heat Transfer 20, 181–314.

Poulikakos, D., Kazmierczak, M., 1987. Forced convection in duct partially filled with a porous material. J. Heat Transfer 109, 653–662.

Vafai, K., Tien, C.L., 1981. Boundary and inertia effects on flow and heat transfer in porous media. Int. J. Heat Mass Transfer 24, 195–203.

Zebib, A., Wo, Y.K., 1985. A two-dimensional conjugate heat transfermodel forced cooling of an electronic block. International Electronic Packaging Conference, Orlando, FL.